Aspects of turbulent/non-turbulent interfaces

By D.K. Bisset, J.C.R. Hunt AND M.M. Rogers

1. Motivation and objectives

A distinct boundary between turbulent and non-turbulent regions in a fluid of otherwise constant properties is found in many laboratory and engineering turbulent flows, including jets, mixing layers, boundary layers and wakes. Generally, the flow has mean shear in at least one direction within the turbulent zone, but the non-turbulent zones have no shear (adjacent laminar shear is a different case, e.g. transition in a boundary layer). There may be purely passive differences between the turbulent and non-turbulent zones, e.g. small variations in temperature or scalar concentration, for which turbulent mixing is an important issue.

The boundary has several major characteristics of interest for the present study. Firstly, the boundary advances into the non-turbulent fluid, or in other words, non-turbulent fluid is entrained. Secondly, the change in turbulence properties across the boundary is remarkably abrupt; strong turbulent motions come close to the non-turbulent fluid, promoting entrainment. Thirdly, the boundary is irregular with a continually changing convoluted shape, which produces statistical intermittency. Its shape is contorted at all scales of the turbulent motion.

When a velocity probe is placed at the edge of a turbulent flow, its output tends to switch back and forth abruptly between a fully turbulent signal and one that is essentially non-turbulent. As discussed by Corrsin & Kistler (1955), this observation was first understood in terms of a sharp convoluted boundary by Corrsin (1943), and Townsend (1948, 1949) made the first measurements of intermittency factor γ (the proportion of time for which the velocity signal is turbulent).

Corrsin & Kistler (1955) also pointed out that irrotational velocity fluctuations are usually found in the non-turbulent flow outside the boundary. Therefore, the boundary marks not an absence of velocity fluctuations but a change in the character of the fluctuations from vortical to irrotational. Since vorticity is transmitted to fluid only through the action of molecular viscosity, there must exist, in conjunction with any boundary region of local velocity gradient, a shear layer that is essentially viscous or laminar in nature. This layer was termed the 'laminar superlayer' by Corrsin & Kistler (1955), and they estimated that its thickness may be as small as the Kolmogorov viscous lengthscale. However, they equated the laminar superlayer to the 'turbulence front', the layer across which all major changes between irrotational and turbulent fluid occur. A more realistic assumption about the thickness of the turbulence front in this sense is that it scales on a characteristic length of vorticity fluctuations — the thickness is not likely to be less than the radius of typical intensely vortical structures. In other words, the turbulent/non-turbulent interface (a present-day synonym for 'turbulence front') is thicker than the laminar superlayer (it is a layer of turbulent fluid), but it is almost always thin compared to the overall turbulent flow dimensions.

In spite of its importance for entrainment, and hence for flow development and scalar mixing, the turbulent/non-turbulent interface (including its vorticity) has not been fully described experimentally, because it is inherently difficult to obtain fully detailed measurements of a thin layer that moves around on a scale much larger than its thickness and faces all different directions. None of the available experimental techniques is able to track the interface position and orientation and to simultaneously measure all velocity components at high resolution. Databases from direct numerical simulations (DNS) of turbulent shear flows at reasonable Reynolds numbers now provide an opportunity to bypass some of the experimental difficulties. In this report the outer boundaries of turbulent zones, defined as the lowest level of vorticity magnitude that can be detected reliably, are delineated in two three-dimensional fields from DNS of far-wakes with different growth rates. Properties of the flow in the vicinity of the vorticity surface are determined through conditional averages, leading to the definition of a fairly distinct turbulent interface region. Some examples of instantaneous flow behavior are examined also. The initial stages of this work were reported by Bisset *et al.* (1998), and a complete account of this research including some implications for RANS modeling is under preparation (Bisset, Hunt & Rogers 1999).

2. Accomplishments

2.1 The data

Two data fields from direct numerical simulations of the far-wake of a parallel flat plate with thick turbulent boundary layers (Moser, Rogers & Ewing 1998) were examined in detail. In these incompressible spectral simulations, data sets from two instants in a prior boundary layer simulation were placed back-to-back (without the walls) at time zero, and then allowed to develop temporally with streamwise and spanwise periodic boundaries. After some time the initial sharp cusps in the mean velocity and turbulence profiles decayed, and the flow then developed in an approximately self-similar manner until the turbulent region became too large for the computational box. One of the simulations was unforced, while weak forcing, in which all two-dimensional modes in the same initial state were magnified at $t = 0$, was applied in the other case; see Moser, Rogers & Ewing (1998) for details. Figure 1 gives an indication of differences in the boundaries of the wake with forcing.

The first data field examined comes from the unforced case, and the second comes from the weakly forced case, at similar times within their self-similar regions. Growth rates and turbulence levels for the two cases are just below (unforced) and just above (forced) typical ranges found in far-wake experiments that do not involve explicit forcing. In both cases the Reynolds number $\dot{m}/\nu$ is 2000 (where $\dot{m}$ is the wake velocity deficit integrated over y), which is high enough for sustained fully-turbulent flow. Results are normalized by U_0, the centerplane mean velocity deficit, and b, the half-mean-velocity width across both sides of the wake. The stored spectral data were projected onto uniform physical grids of $387 \times 400 \times 97$ (unforced) or $387 \times 500 \times 97$ (forced) points for further processing, giving the physical grid data about the same resolution as the spectral.

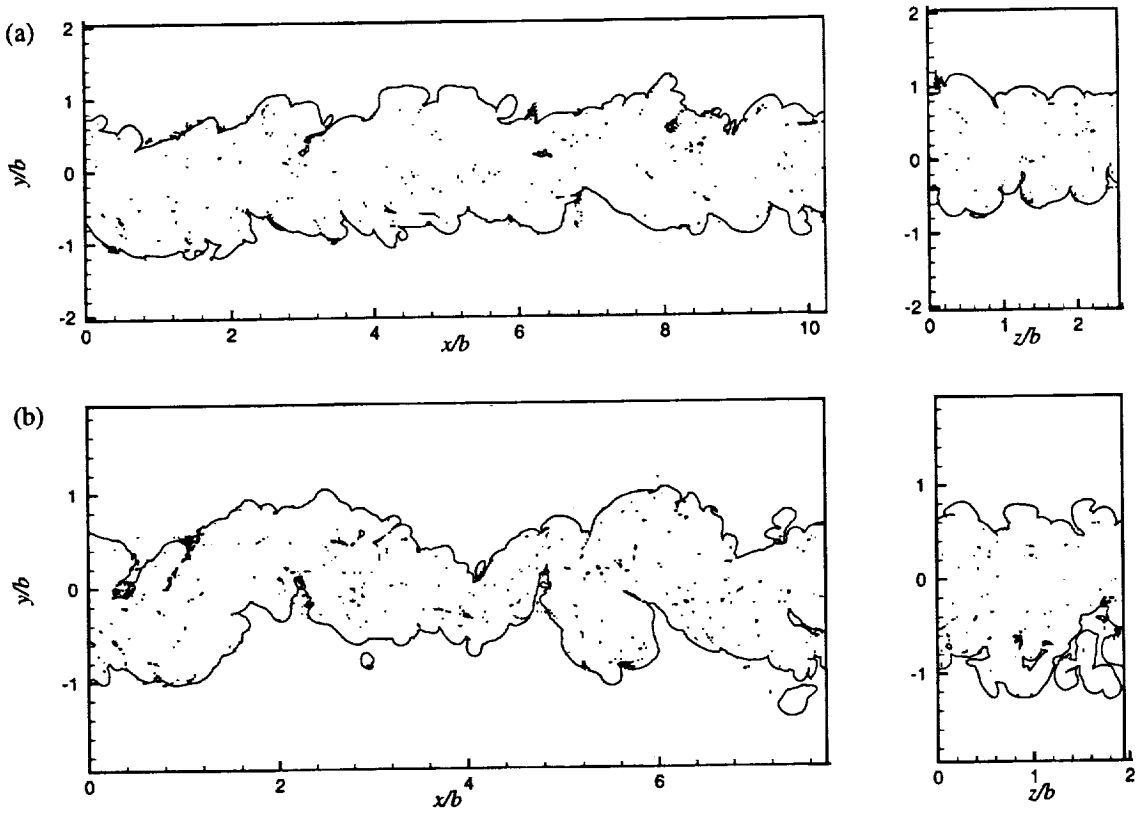

FIGURE 1. Contours of ω in (x, y) and (z, y) planes at the levels used for detection of vorticity surfaces. (a) Unforced wake; (b) weakly forced wake.

A passive scalar quantity T with a Schmidt or Prandtl number of 0.7 was included in the simulations. Its values were 1.0 in the upper free stream and 0.0 in the lower, and it was initialized to a smooth profile across the turbulent region ($T = f(y)$ only). Consequently, the correspondence between non-vortical fluid and free-stream values of the scalar was far from perfect initially, but it improved over time because of mixing within the wake and entrainment of the surrounding fluid. The fact that the two free-stream values are different is very useful for determining the origin (above or below the wake centerplane) of any enclosed or re-entrant region of non-vortical fluid found near the centerplane. A preliminary investigation of the use of scalar levels for detection of the interface is described by Bisset *et al.* (1998).

2.2 Detection of the turbulent/non-turbulent interface

In a fully turbulent flow such as the present, all vortical fluid is expected to be turbulent, and therefore ω, the magnitude of the vorticity vector, can be used for detecting the boundaries of turbulent regions. As with all level-based methods, it is important to set the detection threshold appropriately. In experiments, the combination of free-stream turbulence and instrument noise means that measured

vorticity is often non-zero in true free-stream fluid. In spectral DNS data, background numerical noise has similar consequences (noise in wave-space maps to all physical space). Fortunately, it was determined both by plotting contours and by forming conditional averages from different detection levels that spatial gradients in ω are typically quite steep near the boundary. Therefore, a detection level slightly above the background noise can be used, and the detected interface positions will be almost independent of small changes in that level.

Contours of ω were plotted in several (x, y) and (z, y) planes, and it was found that the contour $\omega = 0.7U_0/b$ best delineated vortical regions in the unforced wake. Below this level, disorganized contours spread out into the free stream; contours above this level tended to fall at very similar positions along the wake edge but also began to find many small low-ω regions throughout the wake interior. Examples of contours at the chosen level in (x, y) and (z, y) planes are shown in Figure 1, for both unforced and forced wakes. Peak ω levels are of order 100 times higher than the chosen level, and the centerplane mean is ten times higher. The same detection level in calculation units was used for the forced wake, although its normalized level $(1.2U_0/b)$ is greater.

Although the indicated surface marks the approximate outer boundary of the turbulent/non-turbulent interface, there is no obvious level of ω that would define an inner boundary, and in fact it may be impossible to define an interface thickness except in a conditionally averaged sense. Note that the detected vorticity *surface* is distinct from the turbulent/non-turbulent interface, a layer of non-zero thickness.

The vorticity surface is quite convoluted and sometimes re-entrant, especially in the forced case (Figure 1). The direction in which the surface faces varies continuously. In a few places there appear to be patches of vortical fluid that are completely isolated, although they are actually two-dimensional cuts through three-dimensional protrusions that are attached to the main body out of the planes shown in the figure.

Conditional averaging through the interface requires not only detections of locations of the interface but also knowledge of the direction in which it is facing at each detected position, because conditional averages would be smeared out very quickly away from the detection point if the averaging path made a random angle to the interface. Therefore, detection positions were separated into groups according to the direction of the normal. Averages were obtained along a fixed direction for each group, the directions used so far being parallel to the x (streamwise), y (transverse) and z (spanwise) axes. In general, data from both sides of the wake were used, with sign reversal where appropriate. The surface at any point was required to face within 25° of the nominal direction except where mentioned.

Vorticity magnitude $\langle\omega\rangle$ conditionally averaged in the y direction for three values of the threshold C_ω is shown in Figure 2 (unforced wake; detections at y_i). For the standard C_ω value (the lowest shown), the proportion of surface area included from each side of the wake, when projected onto the centerplane, is about 26% of centerplane area. In all cases $\langle\omega\rangle$ is almost constant at the same value in the middle part of the wake, and there is a very sharp gradient down through the detection level. There is no restriction on the steepness of this gradient made by the detection

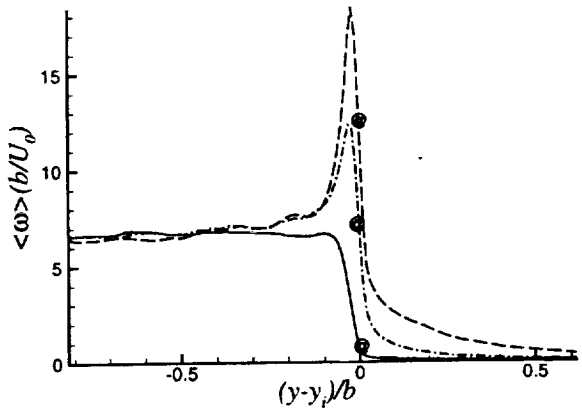

FIGURE 2. Effect of detection threshold C_ω on $\langle\omega\rangle$, unforced wake. Values of $C_\omega b/U_0$ were 0.7, 7.0 and 12.3 at the detection points, indicated by '@'.

process — it just has to be negative. The gradient becomes even steeper with increasing C_ω, but detection points then start to concentrate on locally intense patches of vorticity, reducing the proportion of data accepted and producing sharp peaks in $\langle\omega\rangle$. More significantly, excessive amounts of vortical fluid leak into the irrotational region when C_ω is large. At lower levels of C_ω than shown, numerical noise is detected too often, and irrotational fluid leaks into the vortical region.

It can be inferred from Figure 2 that the average level of ω is constant throughout turbulent zones of the wake, and therefore the conventional distribution of $\overline{\omega}$, with its long tails, is mainly the result of intermittency caused by the wake's convoluted bounding surface. This can be checked by comparing $\overline{\omega}$ with the intermittency distribution (Figure 3). Here the intermittency factor, i.e. the cumulative probability that the surface detection height is greater than y/b, has been rescaled to match $\overline{\omega}$ at the centerplane. Agreement in the shapes of the curves is quite reasonable for both forced and unforced cases. Similar agreement can be expected for other properties that scale with vorticity, such as dissipation rate.

2.3 Possible definition of the turbulent/non-turbulent interface

Conditional averages based on surfaces facing in the x- and z-directions (not shown here), combined with results from the y-direction (e.g. Figure 2), and including results for the passive scalar, lead to the conclusion that vortical fluid is separated from irrotational fluid in all directions by a layer of constant average thickness with strong gradients in both vorticity and scalar. It seems reasonable to call this layer a turbulent/non-turbulent interface, on the grounds that all major transitions from free-stream irrotational fluid to well-mixed vortical fluid occur within its thickness. For the present flows, its thickness (about 6% to 8% of the wake halfwidth) is an order of magnitude larger than the Kolmogorov viscous scale, but several times smaller than the standard deviation of the height of its convolutions. This thickness is fairly similar to the Taylor microscale λ, which could be an attractive choice for an interface scale. However, the validity of scaling with λ cannot

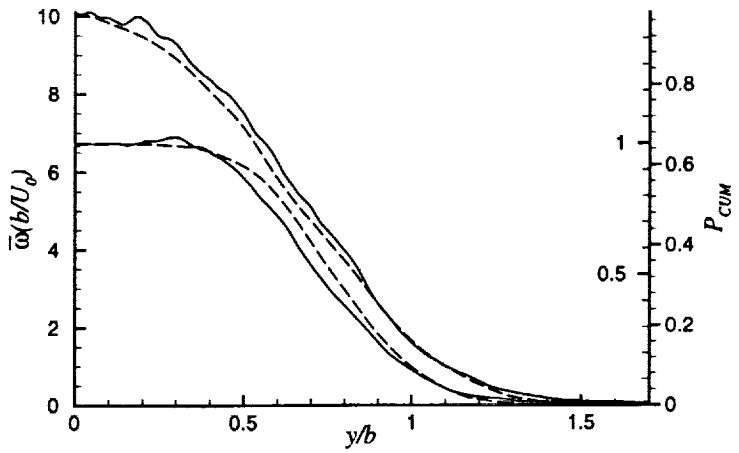

FIGURE 3. Cumulative probability of interface height (----) compared to mean vorticity (———) in the forced (upper curves) and unforced (lower curves) wake. P_{CUM} axes are scaled so that curves match at the centerplane.

be tested until DNS data are available at considerably higher microscale Reynolds numbers. Many properties of the interface such as velocity, velocity fluctuation and vorticity component distributions have been obtained as conditional averages, and will be presented by Bisset, Hunt & Rogers (1999).

2.4 Entrainment

Although entrainment is sometimes thought of as fluid crossing through an interface with a normal component of velocity, entrainment ultimately means that vorticity (and hence the interface) diffuses into irrotational fluid through viscous action (Corrsin & Kistler 1955). The three terms for viscous diffusion of vorticity ($\nu\nabla^2\omega_x$, $\nu\nabla^2\omega_y$ and $\nu\nabla^2\omega_z$) are available from the DNS, and they indicate how vorticity levels are changing within fluid elements irrespective of fluid motion. Symmetry causes cancellations for some relevant terms when conditioned on the ω surface detections, but does not affect the diffusion of spanwise vorticity conditioned on vertically-facing interfaces. This quantity is presented in Figure 4, inverted so that the curve is positive where the magnitude of ω_z is increasing (ω_z is negative here). Figure 4 demonstrates that fluid right at the outer surface of the interface is undergoing the most rapid increase in the magnitude of spanwise vorticity, and at $-0.05b$, within the interface thickness, fluid is losing spanwise vorticity equally rapidly. Thus viscous action is expanding the volume of vortical fluid but also depleting the vorticity of the inner regions. Flows within the vortical regions (e.g. Figure 6) replenish vorticity near the surface. Diffusion of streamwise vorticity is also likely to be significant at vertically-facing interfaces, but cannot be assessed through the present set of detections because ω_x is equally likely positive or negative by symmetry. Entrainment behavior for surfaces facing streamwise and spanwise appears to be similar.

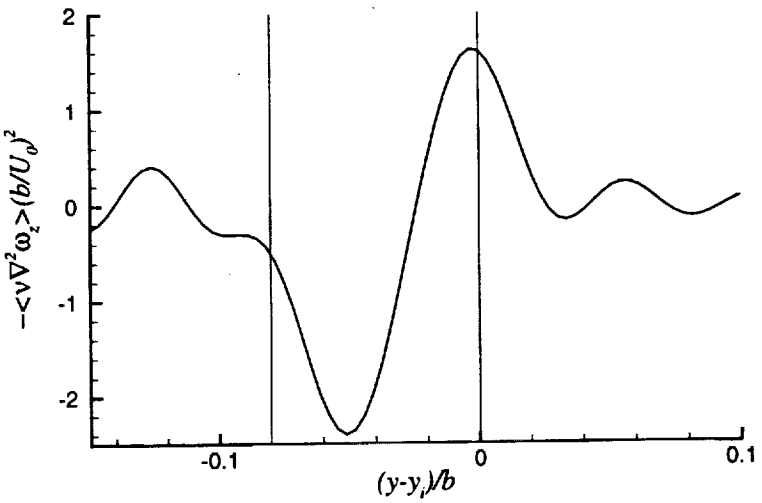

FIGURE 4. Viscous diffusion of ω_z for vertically-facing interfaces, unforced wake. The interface falls approximately between the vertical lines.

2.5 Re-entrant zones

In most places a vertical line passing right through the wake will intersect the vorticity surface twice only, but there are places (especially in the forced wake) where a line passes through more than one distinct vortical zone, intersecting the surface four or even six times. Conceivably a patch of irrotational fluid could be trapped within the wake, but usually the multiple intersections occur within a re-entrant zones, of which several can be identified in Figure 1. Detection of such zones results in sets of three detection positions: the top of the vortical protrusion, the downwards-facing surface where the interface separates protrusion from intrusion, and the bottom of the irrotational intrusion. Conditional averaging is complicated by the variable heights between detections (the protrusions and intrusions have variable thicknesses) that could cause smearing, and therefore conditional averages were calculated separately for the top, middle and bottom detections. No surface angle criteria were used, meaning that the surface normal is often angled well away from the averaging direction (vertical). Re-entrant zones were found either above or below about 7% (16%) of the centerplane area in the unforced (forced) wake.

Composite conditional averages $\langle\omega\rangle$ and $\langle V\rangle$ for re-entrant zones are presented in Figure 5. The '@' indicates detection points on the $\langle\omega\rangle$ curves (Figure 5(a), unforced wake), showing how the curves (including $\langle V\rangle$) from the top and bottom detections have been offset by $+0.2b$ and $-0.12b$ respectively. These offsets were selected for best visual alignment of the curves where they overlap; the offsets were slightly smaller ($+0.16b$ and $-0.1b$) in the forced wake. The $\langle\omega\rangle$ level in the protrusion itself is still remarkably strong given that in some cases the line of conditional averaging is only glancing the tip of the vortical protrusion, and gradients of $\langle\omega\rangle$ through all three interfaces are nearly as steep as in other cases shown already. Results for $\langle\omega\rangle$ with forcing (not shown) are qualitatively the same.

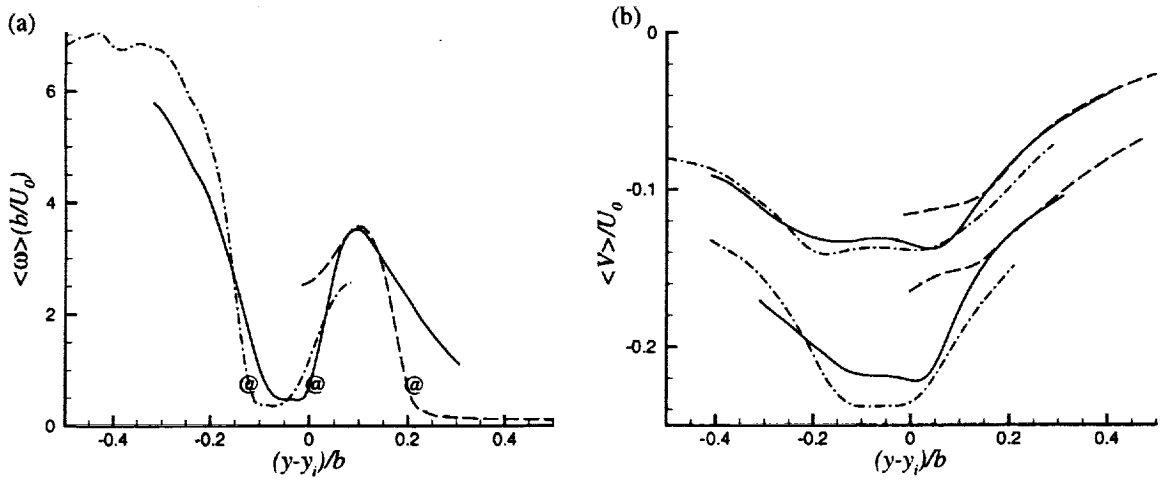

FIGURE 5. Conditional results for re-entrant zones. Surfaces: ---- , outermost; ——— , downwards-facing; —-— , innermost. (*a*) $\langle\omega\rangle$, unforced wake. (*b*) Corresponding distributions of $\langle V\rangle$, unforced (upper curves) and forced (lower curves).

Curves for transverse velocity $\langle V\rangle$, both forced and unforced cases, are given in Figure 5(b). Inwards velocity is very strong for the intruding irrotational fluid, as might be expected, and forcing doubles the speed of intrusion. The streamwise velocity $\langle U\rangle$ (not shown) for all fluid is well below free stream. The most interesting aspect, however, is the large extent of the negative $\langle V\rangle$ region in Figure 5(b): it shows that all of the vortical fluid in the protrusion and the bottom interface is also moving rapidly inwards along with the irrotational fluid. Clearly the re-entrant zone is the result of motion on a larger scale than that of the intrusion itself.

2.6 Maintaining the interface

It appears that local properties of the interface, at least in a conditionally averaged sense, do not vary greatly for different orientations and positions of the interface, and it is clear that the interface maintains its properties over time while entraining fluid into the growing wake (the wake is self-similar with a constant growth rate — see Moser, Rogers & Ewing 1998 for details). Therefore there is likely to be some widespread, perhaps universal, process that maintains the interface in spite of diffusion and mixing processes that would dilute its internal gradients and reduce its surface area. Visualization of individual instants of interfaces in the flow helps to show such aspects of interface structure. Sectional streamlines in flows around interface regions are shown in Figure 6, for part of an (x, y) plane in the forced wake and a (z, y) plane in the unforced wake. These particular realizations were chosen for their relative clarity, but they are not exceptional. Sectional streamlines are lines that are everywhere parallel to velocity vectors projected onto the given plane, and normally the plane of visualization is itself moving at a reference velocity typical of the fluid so that streamlines will emphasize local flow structure. The present reference velocities have been chosen so that a velocity zero (critical

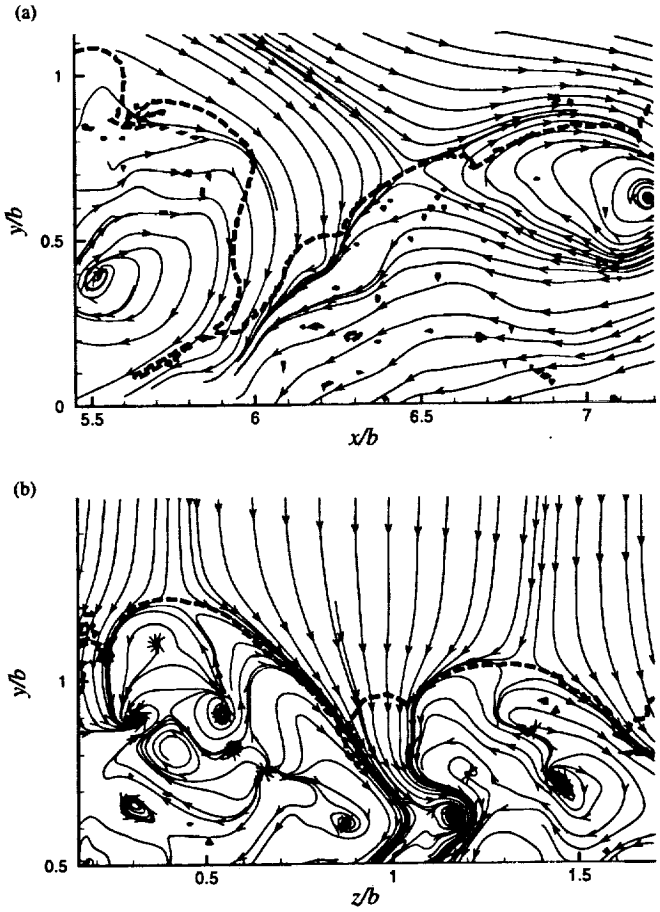

FIGURE 6. Sectional streamlines relative to vorticity surfaces (heavy dashed lines). (*a*) Part of an (x, y) plane, forced wake. (*b*) Part of a (z, y) plane, unforced wake.

point) coincides with the ω surface in a certain area. In fact the exact position of the zero is a free choice, but the resulting pattern of streamlines around the critical point is fully determined by the flow.

In Figure 6(a), (x, y) plane, the zero is clearly a stagnation point (or saddle point) where fast-moving irrotational fluid descends to meet an upflow of vortical fluid. Other zeroes (right at the edges of the figure) are foci within the turbulent fluid upstream and downstream from the saddle, forming a pattern well known from far-wake experiment results both instantaneous and conditionally averaged. In the present DNS, however, the ω surface is resolved too (the heavy dashed line), and it can be seen that fluid accelerates away from the stagnation point in both directions roughly parallel to the interface. Thus well-mixed, vortical fluid and irrotational fluid are brought into close proximity and stretched out along the interface, maintaining gradients across it. The shape of the interface is not static, and in general streamlines that cross the interface indicate the direction of its movement, which includes a downwards push of the re-entrant zone at the present instant. However, the interface does slowly advance into the non-vortical fluid by diffusion of vorticity

(the final stage of entrainment), and an area where the re-entrant zone has previously been almost fully entrained and pinched off can be seen at the bottom left corner of the figure.

A spanwise cut through the wake is shown in Figure 6(b), with the frame of reference velocity (directly upwards) chosen to give a zero at the upper edge of the ω surface. Fortuitously there are two protrusions in this view rising with the same velocity, so stagnation points (saddles) appear on the tops of both. The protrusions are clearly the results of motion on a fairly large scale. Several zeroes appear within the turbulent areas of the protrusions, associated with stable and unstable foci on a smaller scale. As in the (x, y) plane, streams of rising vortical fluid and descending irrotational fluid meet at stagnation points and then accelerate away roughly parallel to the interface. In the center of the figure there appears to be a small bridge of (older?) interface that is being pushed into a deepening fissure.

In summary, cuts through the wake in both directions show how large-scale streams of vortical and irrotational fluid collide at the interface, stretch out along it, and drive its convoluted, fissured shape.

3. Future plans

The work so far has mainly concerned data analysis at isolated instants of time in one basic flow. Work under way or planned will (a) compare the results to theories about free-shear flows, (b) study the implications for RANS modeling, (c) observe entrainment through a time series, and (d) extend to other flows such as boundary layers with pressure gradients, using DNS for both (c) and (d).

REFERENCES

BISSET, D.K., HUNT, J.C.R., CAI, X. & ROGERS, M. M. 1998 Interfaces at the outer boundaries of turbulent motions. *Annual Research Briefs 1998,* Center for Turbulence Research, Stanford University, 125–135.

BISSET, D.K., HUNT, J.C.R. & ROGERS, M.M. 1999 The turbulent/non-turbulent interface bounding a far-wake. *J. Fluid Mech.* (to be submitted)

CORRSIN, S. 1943 Investigation of flow in an axially symmetrical heated jet of air. *NACA WR W-94*, NACA, Washington D.C.

CORRSIN, S. & KISTLER, A.L. 1955 Free-stream boundaries of turbulent flows. *NACA TR 1244*, NACA, Washington D.C.

MOSER, R.D., ROGERS, M.M. & EWING, D.W. 1998 Self-similarity of time-evolving plane wakes. *J. Fluid Mech.* **367,** 255–289.

TOWNSEND, A. A. 1948 Local isotropy in the turbulent wake of a cylinder. *Australian J. Sci. Research, ser. A.* **1(2),** 161–174

TOWNSEND, A. A. 1949 The fully developed turbulent wake of a circular cylinder. *Australian J. Sci. Research, ser. A.* **2(4),** 451–468